X-660-74-255

PREPRINT

NASA TM X- 70750

# SOLAR $He^3$ INFORMATION FROM NUCLEAR REACTIONS IN FLARES

R. RAMATY

B. KOZLOVSKY

(NASA-TM-X-70750) SOLAR He-3: INFORMATION FROM NUCLEAR REACTIONS IN FLARES (NASA) 32 p HC $4.75 CSCL 03B

N74-33252

Unclas

G3/29 48347

AUGUST 1974



GSFC

GODDARD SPACE FLIGHT CENTER

GREENBELT, MARYLAND

# Solar $He^3$: Information from Nuclear Reactions in Flares*

R. Ramaty and B. Kozlovsky

Laboratory for High Energy Astrophysics
NASA-Goddard Space Flight Center
Greenbelt, Maryland USA

*Invited paper presented at the Seminar on Particle Acceleration and Nuclear Reactions in Space, Leningrad, August 19-21, 1974

Abstract

Nuclear reactions can give information on solar $He^3$ in two ways:

1. An upper limit on the photospheric $He^3$ can be set by considering the neutrons produced by nuclear reactions in flares. These neutrons propagate down into the photosphere where they can be captured by protons to produce 2.2 MeV gamma rays. But if the photospheric $He^3/H$ ratio is abou $5 \times 10^{-5}$, only about half the neutrons are captured by protons; the remaining neutrons interact with $He^3$ and produce no gamma rays. The comparison of the 2.2 MeV line with other nuclear lines which are unaffected by $He^3$ yields a photospheric $He^3$ abundance, which, for the presently available gamma-ray observations, is consistent with the $He^3$ abundance in the solar wind.

2. Energetic $He^3$ nuclei in solar particle events have occasionally abundances which greatly exceed the above values or upper limits. We argue that these abundances can be explained by nuclear reactions of flare accelerated particles with the ambient solar atmosphere. However, in order to account for the great variability in the observational data, several assumptions must be made regarding the directionality of the interactions and the acceleration of the nuclei after their production.

1. INTRODUCTION

In the present paper we wish to consider the information on solar $He^3$ that can be obtained from nuclear reactions in flares. We show that gamma-ray observations from solar flares can provide information on the abundance of $He^3$ in the photosphere. The photospheric $He^3$ abundance has not yet been directly determined, and only upper limits exist ($He^3/He^4 < 0.02$, Wallerstein [1]). Measurements in the solar wind (Bame et al. [2] Geiss et al. [3], Geiss [4]) have determined $He^3/He^4$ ratios and thus provide estimates of the photospheric $He^3$ abundance (Geiss and Reeves [5]). But these extrapolations are subject to uncertainties introduced by possible isotopic fractionation which is believed to be the cause of at least some of the variability in the $He^3/He^4$ ratios observed in the solar wind. As we shall show, gamma-ray observations from the flare of 1972, August 4 (Chupp et al. [6]) could provide a direct upper limit to the photospheric $He^3$ abundance of a comparable magnitude to the average $He^3/He^4$ ratio observed in the solar wind, $He^3/He^4 \approx 4x10^{-4}$.

Helium -3 nuclei have also been detected in energetic particle events with $He^3/He^4$ ratios varying over a broad range, from about $10^{-3}$ to 1. In this paper we discuss these observations and the models that could account for them. We show that all the data can probably be explained by nuclear reactions of flare accelerated protons and $\alpha$-particles with the ambient atmosphere provided that various assumptions are made on the directionality of the interacting beams and acceleration of the particles after their production.

## 2. THE PHOTOSPHERIC $He^3$ ABUNDANCE

Information on the photospheric $He^3$ abundance can come from the neutron capture line on hydrogen at 2.23 MeV. This line is formed in the photosphere by fast neutrons which are thermalized and captured by ambient protons to produce deuterons and 2.23 MeV gamma rays. Because the neutrons are also captured by ambient $He^3$, the intensity of the 2.23 MeV line relative to other gamma-ray lines which are unaffected by the $He^3$ abundance gives a measure of the $He^3/H$ ratio in the photosphere.

Fast neutrons are produced by nuclear reactions of accelerated particles in solar flares, most likely in the chromosphere or lower corona (Lingenfelter et al. [7], Lingenfelter and Ramaty [8]). Wang and Ramaty [9] considered in detail the propagation of these neutrons in the solar atmosphere and the subsequent production of gamma rays by the reaction

$$H^1(n,\gamma)H^2. \quad (1)$$

In their treatment a distribution of neutrons was released in the chromosphere or corona, and the path of each neutron after its release was followed by a computer Monte-Carlo simulation. If the neutrons are released above the photosphere, any initially upward moving neutron escapes from the Sun. Some of the downward moving neutrons can also escape after being backscattered elastically by ambient protons, but most of these neutrons either are captured or decay at the Sun. Because the probability for elastic scattering is much larger than the capture probability, the majority of the neutrons are thermalized before they get captured. Since the thermal speed in the photosphere (where most of the captures take place) is much smaller than the speed of light, the gamma-rays from reaction (1) are essentially all at 2.23 MeV and the Doppler-broadened width of this line is negligible.

The bulk of neutrons at the Sun are captured either on H or on $He^3$. Whereas capture on H yields a 2.2 MeV photon, capture on $He^3$ proceeds via the radiationless transition

$$He^3(n,p)H^3, \quad (2)$$

and hence produces no photons. The cross sections for reactions (1) and (2) are $\sigma_c(H) = 2.2 \times 10^{-30}\ \beta^{-1}\ cm^2$ and $\sigma_c(He^3) = 3.7 \times 10^{-26}\ \beta^{-1}\ cm^2$, respectively, where $\beta$ is the velocity of the neutron (for details see Wang and Ramaty [9]). Thus, if the $He^3/H$ ratio in the photosphere is $\sim 5 \times 10^{-5}$ comparable to that observed in the solar wind, nearly equal numbers of neutrons are captured on $He^3$ as on H.

The results of the Monte-Carlo calculations of Wang and Ramaty [9] are presented in Figures 1 and 2 for two assumptions on the photospheric $He^3$ abundance: $He^3/H = 0$ and $He^3/H = 5 \times 10^{-5}$. In these calculations an isotropic distribution of monoenergetic neutrons of energy $E_n$ is released above the photosphere. The solid lines are the probabilities for the various indicated processes. As can be seen, the capture and loss probabilities increase with increasing energy, because higher energy neutrons penetrate deeper into the photosphere. This reduces their escape probability and leads to a shorter capture time, thereby reducing the decay probability. When $He^3/H = 5 \times 10^{-5}$, the probability for loss on $He^3$ almost equals the capture probability on protons. The escape probability is greater than 0.5, because all initially upward moving neutrons escape from the Sun. Note that the sum of all probabilities equals 1.

The dashed lines in Figures 1 and 2 are photon yields per neutron, $f(\theta, E_n)$, for various neutron energies, $E_n$, and angles, $\theta$, between the earth-sun line and the vertical to the solar surface. The function f is defined such that for an average neutron production rate, q, the average 2.23 MeV photon flux at Earth is

$$\phi\ (2.2\ \text{MeV}) = qf/(4\pi R^2) \tag{3}$$

where R = 1 A.U..

At low neutron energies and $\theta$ near zero, f is close to the capture probability on protons. This means that gamma rays from low-energy neutrons observed close to the vertical escape essentially unattenuated from the Sun. At higher energies and at larger angles, however, there is significant attentuation of the gamma rays due to Compton scattering in the photosphere. Even though f does depend on $E_n$, for flares sufficiently close to longitude and latitude zero on the Sun and neutron energies between about 1 and 100 MeV, we can approximate it by a constant. Most of the neutrons have energies in this range [8]. Thus, for $He^3/H \sim 5 \times 10^{-5}$ we use $f \simeq 0.12$, and for $He^3/H \simeq 0$, we take $f \simeq 0.2$. Note that these approximations are quite valid for the flare of 1972, August 4, since its solar longitude and latitude were E08 and N14.

By using these results, we can obtain a relationship between the photon yield f and the photospheric $He^3/H$ ratio:

$$f \simeq 0.2\left[1 + \frac{\sigma_c(He^3)}{\sigma_c(H)} \left(\frac{He^3}{H}\right)\right]^{-1} . \qquad (4)$$

The strongest gamma-ray lines from solar flares are expected at 2.23, 0.51, 4.43, 6.14, 0.48 and 0.43 MeV, resulting from neutron capture on hydrogen, positron annihilation, and deexcitation of excited states in $C^{12}$, $O^{16}$, $Li^{17}$ and $Be^7$, respectively. Ramaty and Lingenfelter [10] have recently updated the calculations on the production of these lines in both the thin and thick-target interaction models. For the composition of the ambient solar atmosphere they have used the abundances given by Cameron [11], i.e. H:He:CNO = 1:0.07:0.0012. For the accelerated particle populations they considered power-law and exponential spectra. In the thin-target model these are

$$N_i(E) = k_i E^{-s} \quad (5)$$

and

$$N_i(P) = k_i' \exp(-P/P_o), \quad (6)$$

respectively. Here $N_i(E)$ and $N_i(P)$ are the instantaneous numbers of accelerated particles of kind i in the interaction region per unit energy per nucleon, E, or unit rigidity, P; $k_i$ and $k_i'$ are constants determined by normalizing the $N_i$'s to 1 proton of energy greater than 30 MeV and by using the composition of the ambient solar atmosphere; and s and $P_o$ are, respectively, the spectral index and characteristic rigidity assumed to be the same for all accelerated particle components. In the thick-target model they used expressions similar to equations (5) and (6), but they replaced the instantaneous numbers $N_i$ by the total number of accelerated particles released from the flare region downward into the Sun. As with the instantaneous fluxes, these are normalized by using the composition of the ambient solar atmosphere.

The calculated ratios of the yield of the excited nucleus $C^{12*4.43\,MeV}$ to the neutron yield for both the thin and thick-target models are shown in Figure 3 as functions of s, for power-law spectra, and $P_o$, for exponential spectra. By comparing the results of Figure 3 with data on the observed ratio of the intensity of the 4.43 MeV line to that of 2.23 MeV line, it is possible to deduce the spectral index of the accelerated particles in the flare region for various assumed

$He^3/H$ ratios. We have that

$$\left(\frac{C^{12*4.43}}{n}\right) = \frac{\phi_{4.43}}{\phi_{2.23}} f \qquad (7)$$

where $C^{12*4.43}/n$ is the quantity plotted in Figure 3, and $\phi_{4.43}/\phi_{2.23}$ is the observed ratio of the 4.43 and 2.23 MeV line intensities. According to Chupp et al. [12], for the 1972, August 4 flare, $\phi_{4.43}/\phi_{2.23} = 0.11 \pm 0.04$. The resultant spectral parameters are shown in Table 1.

TABLE 1

Deduced spectral parameters for the flare of 1972, August 4 for various photospheric $He^3/H$ ratios

| | Thin Target | | Thick Target | |
|---|---|---|---|---|
| $He^3/H$ | S | $P_o$(MV) | S | $P_o$(MV) |
| 0 | 2.2-1.9 | 125-200 | 3.2-2.9 | 85-135 |
| $5x10^{-5}$ | 1.9-1.6 | 180-285 | 2.9-2.5 | 125-225 |
| $10^{-4}$ | 1.8-1.5 | 235-360 | 2.7-2.3 | 170-290 |
| $1.4x10^{-4}$ | 1.7-1.4 | 260-410 | 2.6-2.2 | 200-335 |

As can be seen, in order to account for the observed $\phi_{4.43}/\phi_{2.23}$ ratio, an increasing $He^3/H$ requires accelerated particles with harder energy spectra (larger $P_o$ or smaller s). This result is due to the fact that as the $He^3$ abundance increases, the larger neutron absorption in the photosphere has to be compensated by a larger neutron production relative to the 4.43 MeV photon production; and this can be achieved by a harder particle spectrum because the neutron production cross section increases with increasing particle energy as opposed to the decrease of the 4.43 MeV excitation cross section.

A limit on the photospheric $He^3/H$ could be set if a limit existed on the hardness of the accelerated particle spectrum. This information, however, is not available from charged particle observations, because of difficulties in deducing the spectrum of the flare accelerated particles in interplanetary space (see [10]). A limit on the hardness of the particle spectrum, nonetheless, can be obtained from observations of gamma rays which are produced from the decay of $\pi$-mesons. Positive pions produce positrons which can annihilate into 0.51 MeV photons, and neutral pions annihilate into high energy ($\sim$ 70 MeV) gamma rays.

In Figures 4 and 5 we show the calculated 0.51 MeV line intensity, $\phi_{0.51}$, for various $He^3/H$ ratios for the thin and thick-target models and power-law and exponential spectra. In these figures, $\phi_{0.51}$ is calculated for positrons from $\pi^+$ decay only; it is also assumed that one half of the positrons escapes from the Sun and the other half annihilates. Because in solar flares positrons can also result from the decay of radioactive nuclei and $e^+$-$e^-$ pairs produced by electrons [10], $\phi_{0.51}$ is a lower limit on the total flux of positron annihilation radiation. The comparison of the data of Chupp el al. [12] with the calculations, therefore, yields upper limits on $He^3/H$. In the thin-target model $(He^3/H) < 3.5 \times 10^{-5}$ and in the thick-target model $(He^3/H) < 6.5 \times 10^{-5}$. Both these upper limits are for the exponential spectrum. The power-law spectrum appears to predict a larger 0.51 MeV intensity than observed. It should be noted, however, that these upper limits are obtained by assuming that only one half of the positrons escape from the Sun. If a larger fraction of the positrons escape, or if some of the positrons are trapped in a low density ($< 10^{12} cm^{-3}$) region at the Sun, then the ratio $He^3/H$ could be larger than the values given above.

Let us consider now the gamma rays from $\pi^\circ$ decay. In Figure 6 we show the yields of $\pi^\circ$ mesons per neutron, calculated in the thin and thick-target models for power-law and exponential spectra using the $\pi^\circ$ production cross sections in pp and p$\alpha$ reactions [13]. From these calculations and the results of Table 1 we obtain the high-energy ($\sim$ 70 MeV) photon flux at Earth for various $He^3/H$ ratios.

The results are shown in Figure 7 and 8 for the thin and thick-target models, respectively. Here $\phi_{\pi^\circ}$ is the total photon flux from $\pi^\circ$ decay. The energy spectrum of these photons depends on the spectrum of the primary particles, but most of them have energies greater than about 30 MeV.

Unlike in the case of $\pi^+$ decay, there are no inherent uncertainties in the calculation of $\phi_{\pi^\circ}$. The problem here is due to the lack of high energy gamma ray data from solar flares. Therefore, all we can do at the present time is to give the values of $\phi_{\pi^\circ}$ that would have been obsevED from the 1972, August 4 flare for various values of $He^3/H$. From Figures 7 and 8 we obtain that if $He^3/He^4 = 4 \times 10^{-4}$, as observed on the average in the solar wind, and if $He/H = 0.07$ then:

$$\begin{aligned}
0.01 \le \phi_{\pi^\circ} \le 0.16 &\text{ for the thick-target exponential model,} \\
0.06 \le \phi_{\pi^\circ} \le 0.27 &\text{ for the thin-target exponential model,} \\
0.23 \le \phi_{\pi^\circ} \le 0.42 &\text{ for the thick-target power-law model,} \\
0.42 \le \phi_{\pi^\circ} \le 0.7 &\text{ for the thin-target power-law model.}
\end{aligned} \tag{8}$$

These fluxes are quite large and could have been detected if proper instrumentation had been flown during the flash phase of the 1972, August 4 flare.

## 3. $He^3$ IN SOLAR PARTICLE EVENTS

Having discussed the abundance of $He^3$ in the photosphere as derived from the gamma ray data, we proceed now to investigate energetic solar particle events since some of these were found to be quite abundant in $He^3$.

Energetic $He^3$ nuclei of solar origin were detected on several occasions [14, 15, 16, 17, 18, 19, 20, 21]. In these measurements, the observed $He^3/H^1$ and $He^3/He^4$ ratios vary from event to event; they also vary with energy in some events, but are relatively constant in others.

A flare which produced both $He^3$ and $H^2$, and the observed (Webber et al. [19]) $He^3/He^4$ ratio was the lowest among the above measurements, was the event of 1972, August 4. As discussed above, this flare also produced gamma-ray lines, which clearly indicates that nuclear reactions did take place in the flare region.

The $He^3/He^4$ data for the flare of 1972, August 4 are shown by the solid points in Figure 9, together with the calculated $He^3/He^4$ ratios in the thin-target model (Ramaty and Kozlovsky [22]). The parameter $x_1$ is the amount of matter traversed by relativistic particles in this model. As can be seen, the data fit the calculations quite well if $x_1 \simeq 1.5$ g cm$^{-2}$; this amount of matter is consistent with the assumption of a thin target because it allows the primary particles that produce the $He^3$ nuclei to escape from the interaction region without losing a large fraction of their energy.

The open data points in Figure 9 are the data of Hsieh and Simpson [15] obtained by summing over 7 solar particle events. As can be seen, in order to account for these data in the thin-target model, $x_1$ has to be at least 4 g $cm^{-2}$, and this target thickness is not consistent with the assumption of a thin target because the primary protons and $\alpha$-particles which produce the observed $He^3$ can no longer escape from the interaction region. This indicates that there are flares in which more $He^3$ is produced than expected in a simple thin-target model.

In addition to the above data, there are several events in which very large $He^3/H^1$ and $He^3/He^4$ ratio were observed. These occurred on May 28, 1969 [21], October 14, 1969 [18], and July 30, 1970 [20]. The data is summarized in Table 2.

TABLE 2

Data for $He^3$-rich Events

| Date | $He^3/H^1$ | $He^3/He^4$ | $He^4/H^1$ | $He^3/H^2$ | Energy Range |
|---|---|---|---|---|---|
| 1969, May 28 | 0.6 | 1.5 | 0.4 | >250 | 4-80 MeV/nucl |
| 1969, Oct. 14 | $3 \times 10^{-3}$ | 0.3 | $10^{-2}$ | >10 | 5-20 MeV/nucl |
| 1970, July 30 | 0.10 | 0.54 | 0.2 | >20 | ~10-20 MeV/nuc |

We first note that in these $He^3$-rich events, $He^3$ is much more abundant than $H^2$; but if the $He^3$ were produced in nuclear reaction of accelerated particles, $He^3$ and $H^2$ should have similar abundances. In order to overcome this difficulty, in a previous paper [22] we considered the production of $H^2$ and $He^3$ in a thick-target model where the products of the nuclear reactions are observed in the backward hemisphere with respect to the direction of the primary beam. Because $H^2$ is emitted predominantly into the forward hemisphere whereas $He^3$ is distributed almost isotropically, the $He^3/H^2$ ratio in the backward hemisphere is enhanced above its average value.

In figures 10 and 11 we show the calculated $He^3/H^2$ ratios in the backward hemisphere in the thick-target model for power-law and exponential spectra, respectively. As can be seen, the $He^3/H^2$ ratio can be as high as 40, a value larger than the observed lower limits on $He^3/H^2$ given in Table 2 for the 1969, October 14 and 1970, July 30 events. This is not the case for the 1969, May 28 event but we note that for this event not only deuterium is suppressed but also the protons; we shall discuss a possible reason for these additional suppressions below.

The calculated $He^3/H^2$ ratios assume high values at low energies ($\lesssim$ 1 MeV), whereas the observed $He^3/H^2$ ratios are large also at higher energies. Therefore, some acceleration of the isotopes must occur after their production. The need for post-production acceleration also follows from the fact that the $He^3$ nuclei at the observed energies have much shorter stopping ranges than the path length required for their production [27]. Alternatively, in the thick-target model, the $He^3$ nuclei emitted in the backward direction probably have to go through a path length equal to the stopping range of the primary downward moving protons. Because these $He^3$ nuclei are produced by protons in the range 50 to 200 MeV, this path length is about 1 to 10 g $cm^{-2}$. Since this range of values is much larger than the stopping length of the low energy $He^3$ nuclei, post production acceleration is again required.

In addition to the large $He^3/H^2$ ratios, $He^3$-rich events also have large $He^3/H^1$ and $He^3/He^4$ ratios. The energy spectra of the $H^1$, $He^3$, and

$He^4$, however, appear to be quite similar [21], indicating that these nuclei are probably accelerated by the same mechanism. Because the observed $He^3/H^1$ and $He^3/He^4$ ratios are much larger than in the ambient medium, the postulated acceleration mechanism cannot simply accelerate ambient material; and even if the accelerator would accelerate preferentially according to Z/A, it still could not account for the observations, because it would enhance the $He^3/He^4$ ratio but depress the $He^3/H^1$ ratio contrary to the observed data which shows that both $He^3/H^1$ and $He^3/He^4$ are enhanced.

Acceleration of the ambient medium can be avoided if the acceleration mechanism requires an injection threshold. Such a threshold may be required in a dense medium where at low energies fast particles suffer large energy losses and hence cannot be efficiently accelerated. The $He^3$ nuclei could acquire their injection energy from nuclear reactions; and because $H^3$ is not detected, we should observe particles injected predominantly into the backward direction with respect to the primary beam. The $H^1$ and $He^4$ nuclei could then be injected by backward elastic scatterings and possibly by mirroring or scattering in magnetic fields.

The details of the angular distributions of protons and alpha particles from such scatterings have not yet been worked out, but preliminary estimates show that events such as that of 1969, October 14 can be understood in terms of backward injection of $H^1$, $He^3$ and $He^4$. In the 1969, May 28 event, in addition to the enrichment of $He^3$ there is also a depletion of $H^1$. This effect cannot be caused by backward elastic scattering because it is easier to backscatter protons than $\alpha$-particles.

It may be that in this case we see nuclei which have been produced at an exceptionally great depth in the solar atmosphere ($\gtrsim$ 10 g cm$^{-2}$). This depth is sufficiently large to disperse the backward moving protons by elastic scattering on ambient $He^4$, and hence suppress their acceleration. The same effect could further suppress the $H^2$ but leave the $He^3$ and $He^4$ essentially unaffected. The correlation seen in Table 2 between the enhancement of $He^3$ and suppression of $H^1$ and $H^2$ is consistent with this qualitative idea.

## 4. SUMMARY

The abundance of ambient $He^3$ in the solar atmosphere, $He^3/H^1$ is on the order of a few times $10^{-5}$. This result comes from the observed composition of the solar wind, and from gamma-ray observations which provide direct information on the photospheric abundance. We have discussed in detail the considerations that go into the gamma-ray method. The presently available data shows no discrepancy between the photospheric and solar wind abundances. But future simultaneous measurements of gamma ray lines at 2.2 and 4.4 MeV and gamma rays above 30 MeV could improve the photospheric $He^3$ determination to a point where possible differences between the solar wind and photosphere could become detectable.

The abundance of $He^3$ nuclei in energetic solar particle events is larger than the ambient abundances on all occasions when such nuclei were detected. Because of the observation of nuclear gamma-ray lines, we now know that nuclear reactions do take place in flares, and these reactions are probably responsible for the production of energetic $He^3$ nuclei as well. There are however, several effects which complicate this interpretation of the data.

1. The absence of deuterium and tritium in $He^3$-rich events can probably be explained by directional kinematics. These nuclei are emitted preferentially in the forward hemisphere with respect to the direction of the primary particle and hence they are not observed in the direction in which particles escape from the Sun.

2. $He^3$-rich events show enhanced $He^3$ up to several tens of MeV/nucleon, and, moreover, the $H^1$, $He^3$ and $He^4$ have quite similar energy spectra. This suggests that a common accelerating mechanism is affecting these nuclei. Because the ambient medium is not accelerated, the acceleration should require an injection mechanism which could be the nuclear reactions themselves for $He^3$, and elastic or magnetic scatterings for $H^1$ and $He^4$.

3. At least one $He^3$-rich flare shows a larger suppression of protons and deuterons than expected from the above ideas. We suggested that this suppression could be due to dispersion during acceleration caused by elastic scatterings with ambient nuclei. Because such dispersion is caused by target nuclei heavier than the projectile, it would effect mainly the protons and deuterons and not the $He^3$ and $He^4$ nuclei. Tritium, however, could also be destroyed by nuclear reactions.

The following qualitative predictions emerge from our discussion. There should be a correlation between enrichment of $He^3$ and depletion of $H^1$ and $H^2$. In particular, events in which $He^3$ is only moderately enriched should show a measurable flux of $H^2$. Boron should be observed in $He^3$-rich events, with a B/C ratio comparable to or perhaps somewhat smaller than the $He^3/He^4$ ratio. Nuclear gamma rays should also be observed from $He^3$-rich flares.

References


(1) Wallerstein, G. 1968, Nucleosynthesis, Edited by W. D. Arnett, C. J. Hansen, J. W. Truran and A. G. W. Cameron, Gordon and Breach, N.Y. p. 2

(2) Bame, S. J., Hundhausen, A. J., Asbridge, J. R., and Strong, I. B. 1968, Phys. Rev. Letters, 20, 393.

(3) Geiss, J., Eberhardt, P., Buhler, F., Meister, J., and Signer, P. 1970, J. Geophys. Res. 75, 5972.

(4) Geiss, J. 1972, Solar Wind, Edited by C. P. Sonett, P. J. Coleman and J. M. Wilcox (NASA SP-308), p. 559.

(5) Geiss, J. and Reeves, H. 1972, Astron. and Astrophys. 18, 120.

(6) Chupp, E. L., Forrest, D. J., Higbie, P. R., Suri, A. N., Tsai, C., and Dunphy, P. P. 1973, Nature 241, 333.

(7) Lingenfelter, R. E., Flamm, E. J., Canfield, E. H., and Kellman, S. 1965, J. Geophys. Res., 70, 4077.

(8) Lingenfelter, R. E., and Ramaty, R. 1967, High Energy Nuclear Reactions in Astrophysics, Editedby B. S. P. Shen (W. A. Benjamin, New York), p. 99.

(9) Wang, H. T. and Ramaty, R. 1974, Solar Physics, 36, 129.

(10) Ramaty, R. and Lingenfelter, R. E. 1974, Proceedings of the Joint IAU-COSPAR Symposium No. 68 on Solar γ, X, and EUV Radiation, Buenos Aires, June 1974 (in press).

(11) Cameron, A. G. W. 1973, Space Sci. Rev. 15, 121.

(12) Chupp, E. L., Forrest, D. J., Suri, A. N. 1974, Proceedings of the Joint IAU-COSPAR Symposium No. 68 on Solar γ, X and EUV Radiation, Buenos Aires, Argentina, June 1974 (in press).

(13) Stecker, F. W., 1970, Astrophys. and Space Science 6, 377, 1970.

(14) Schaeffer, O. A., and Zahringer, J. 1962, Phys. Rev. Letters, 8, 389.

(15) Hsieh, K. C., and Simpson, J. A. 1970, Astrophys. J. Letters, 162, L191.

(16) Dietrich, W. F. 1973, Ap. J., 180, 955.

(17) Anglin, J. D., Dietrich, W. F., and Simpson, J. A. 1973 High-Energy Phenomena on the Sun, Symposium Proceedings, Edited by R. Ramaty and R. G. Stone (NASA SP-342), p. 315.

(18) Garrard, T. L., Stone, E. C., and Vogt, R. E. 1973, High Energy Phenomena on the Sun, Symposium Proceedings, edited by R. Ramaty and R. G. Stone (NASA SP-342), p. 341.

(19) Webber, W. R., Roelof, E. C., McDonald, F. B., Teegarden, B. J. and Trainor, J. 1974 (preprint).

(20) Anglin, J. D., Simpson, J. A. and Zamow, R. 1974, Bull. Amer. Phys. Soc. 19, 457.

(21) Balasubrahmanyan, V. K. and Serlemitsos, A. T. 1974, Submitted to Nature.

(22) Ramaty, R. and Kozlovsky, B. 1974, Ap. J., in press.

Figure Captions

1. Probabilities for neutron escape, decay, and capture in the solar atmosphere (solid lines), and photon yields per neutron (dashed lines) for no $He^3$ in the photosphere.
2. Probabilities for neutron escape, decay and capture in the solar atmosphere (solid lines), and photon yields per neutron (dashed lines) for $He^3/H = 5x10^{-5}$.
3. Ratios of the $C^{12*4.43}$ yield to the total neutron yield for the thin and thick-target models, and power law and exponential spectra.
4. The flux of 0.51 MeV photons from $\pi^+$ decay for the 1972, August 4 flare as a function of the photospheric $He^3/H$ ratio calculated in the thin-target model for power-law and exponential spectra. The error bar indicates the measured flux.
5. The flux of 0.51 MeV photons from $\pi^+$ decay for the 1972, August 4 flare as a function of the photospheric $He^3/H$ ratio calculated in the thick-target model for power-law and exponential spectra. The error bar indicates the measured flux.
6. Ratios of the $\pi^\circ$ yield (multiplied by 2) to the neutron yield for the thin and thick-target models and power law and exponential spectra.
7. The flux of gamma rays from $\pi^\circ$ decay for the 1972, August 4 flare as a function of the photospheric $He^3/H$ ratio calculated in the thin-target model for power-law and exponential spectra. The spectral parameters given in Table 1 are also shown in the figure. There is no observational data for $\phi_{\pi^\circ}$.

8. The flux of gamma rays from $\pi^o$ decay for the 1972, August 4 flare as a function of the photospheric $He^3/H$ ratio calculated in the thick-target model for power-law and exponential spectra. The spectral parameters given in Table 1 are also shown in the figure. There is no observational data for $\phi_{\pi^o}$.
9. The $He^3/He^4$ ratio at the same kinetic energy per nucleon in the thin-target model for various spectral indexes s.
10. The $He^3/H^3$ ratio at the same kinetic energy per nucleon in the backward hemisphere calculated in the thick-target model with power law spectra with various spectral indexes s.
11. The $He^3/H^2$ ratio at the same kinetic energy per nucleon in the backward hemisphere calculated in the thick-target model with exponential spectra with various values of $P_o$.

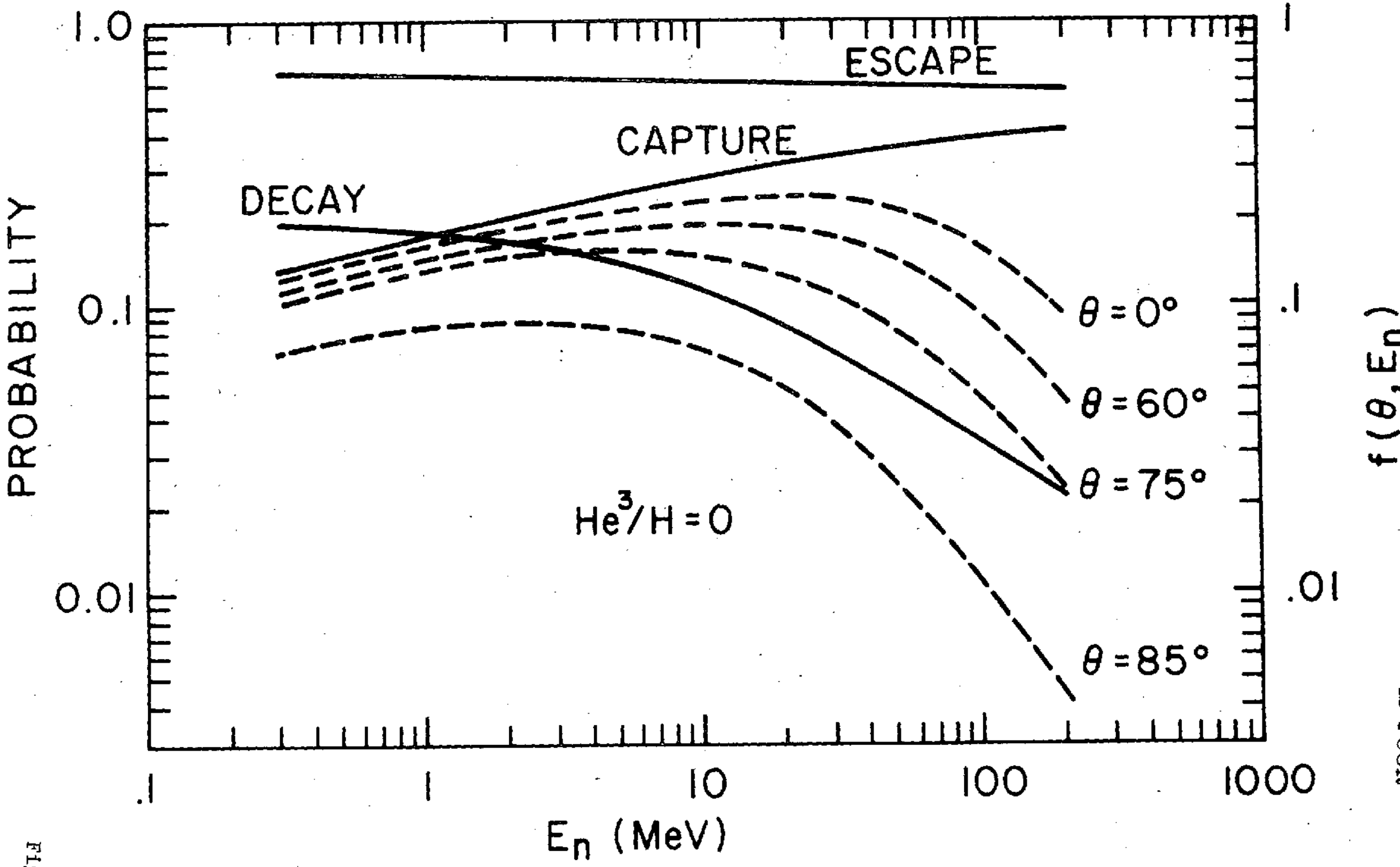

PROBABILITY
1.0
0.1
0.01
ESCAPE
CAPTURE
DECAY
θ = 0°
θ = 60°
θ = 75°
θ = 85°
He³/H = 0
.1
1
10
100
1000
En (MeV)
f(θ, En)


Figure 1

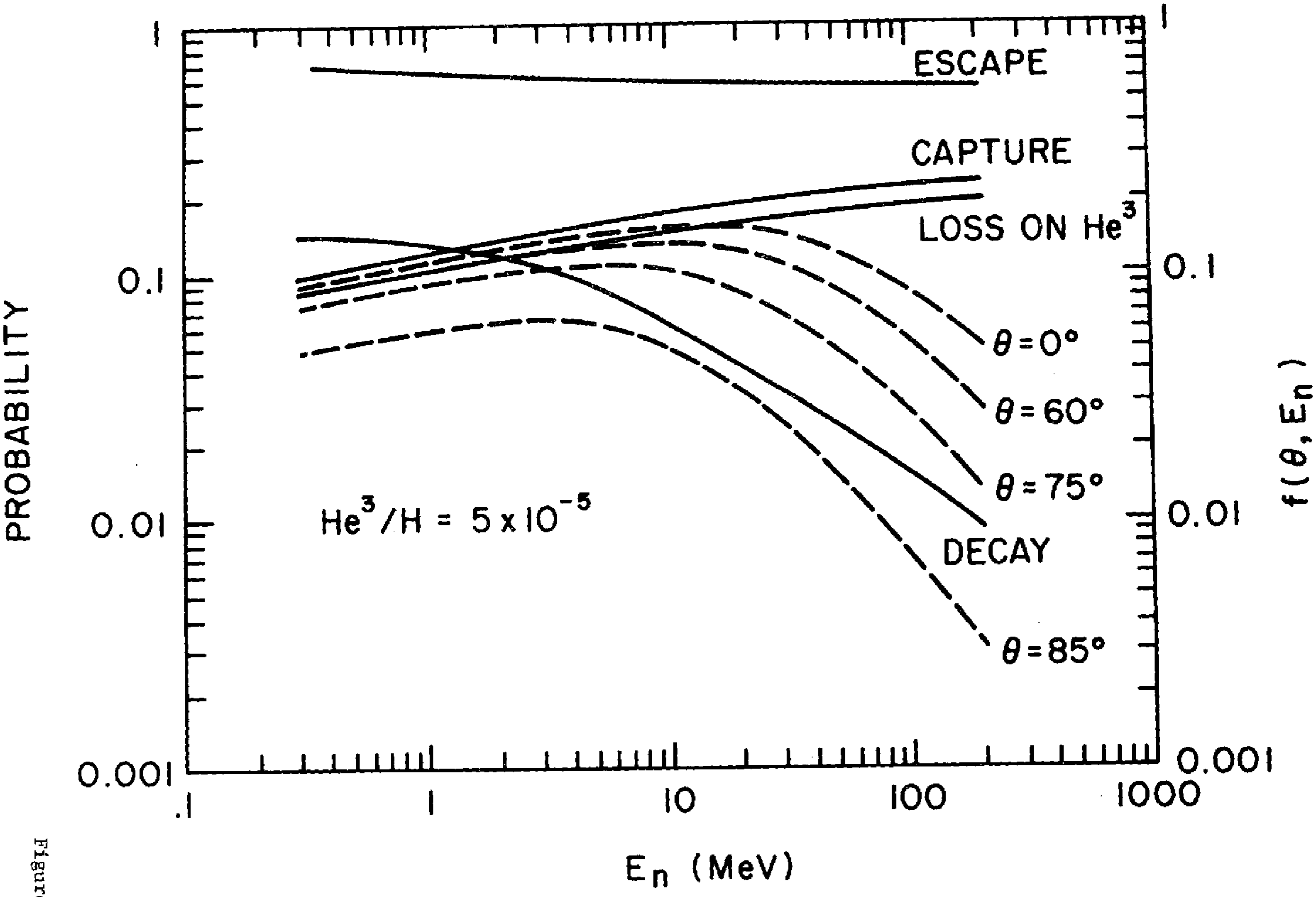
ESCAPE
CAPTURE
LOSS ON He3
θ=0°
θ=60°
θ=75°
DECAY
θ=85°
He3/H = 5 x 10-5
PROBABILITY
f(θ, En)
En (MeV)
1
0.1
0.01
0.001
.1
1
10
100
1000

Figure 2

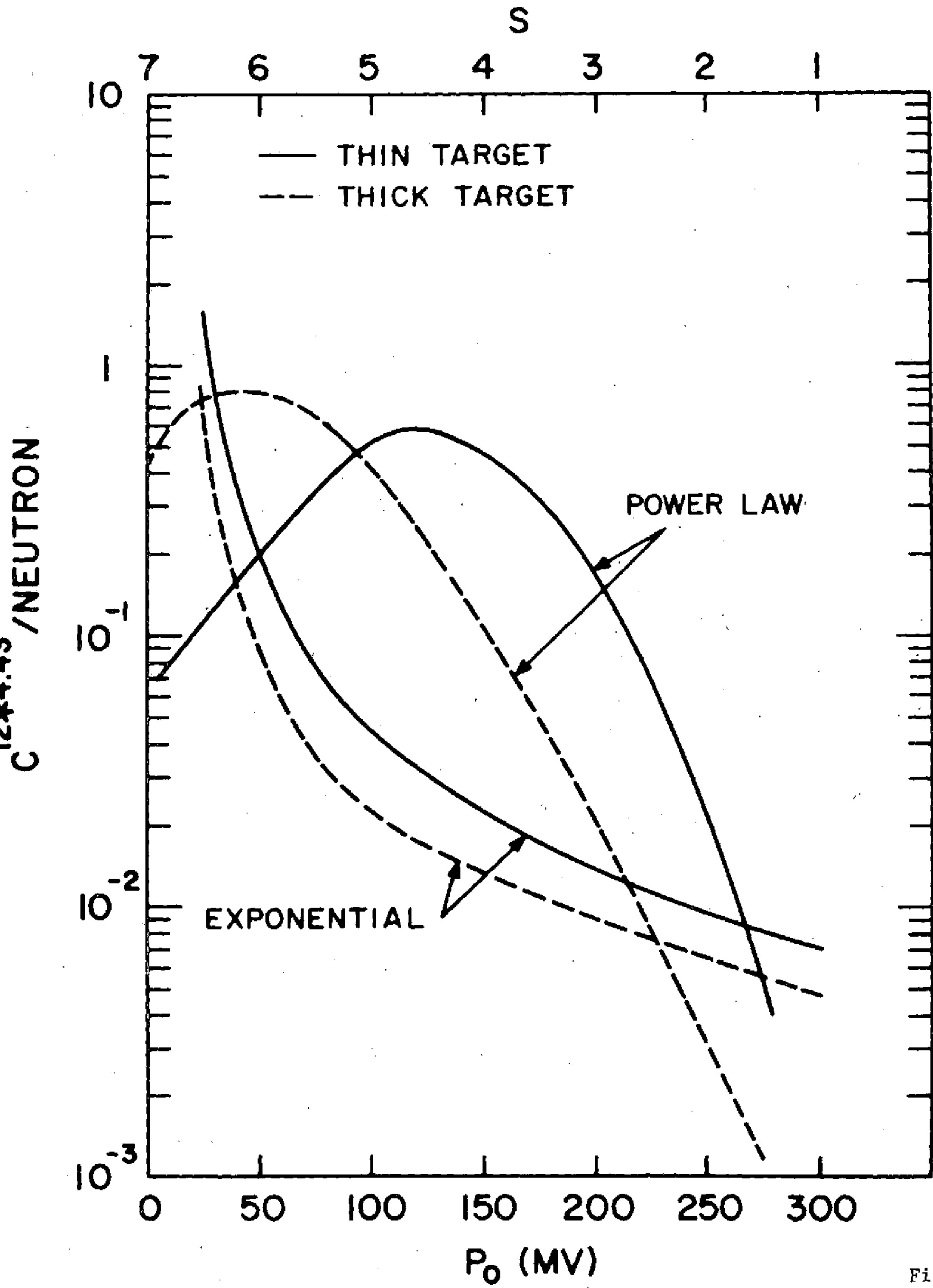
S
7
6
5
4
3
2
1
10
1
$10^{-1}$
$10^{-2}$
$10^{-3}$
THIN TARGET
THICK TARGET
POWER LAW
EXPONENTIAL
$C^{12*4.43}$/NEUTRON
0
50
100
150
200
250
300
$P_0$ (MV)

Figure

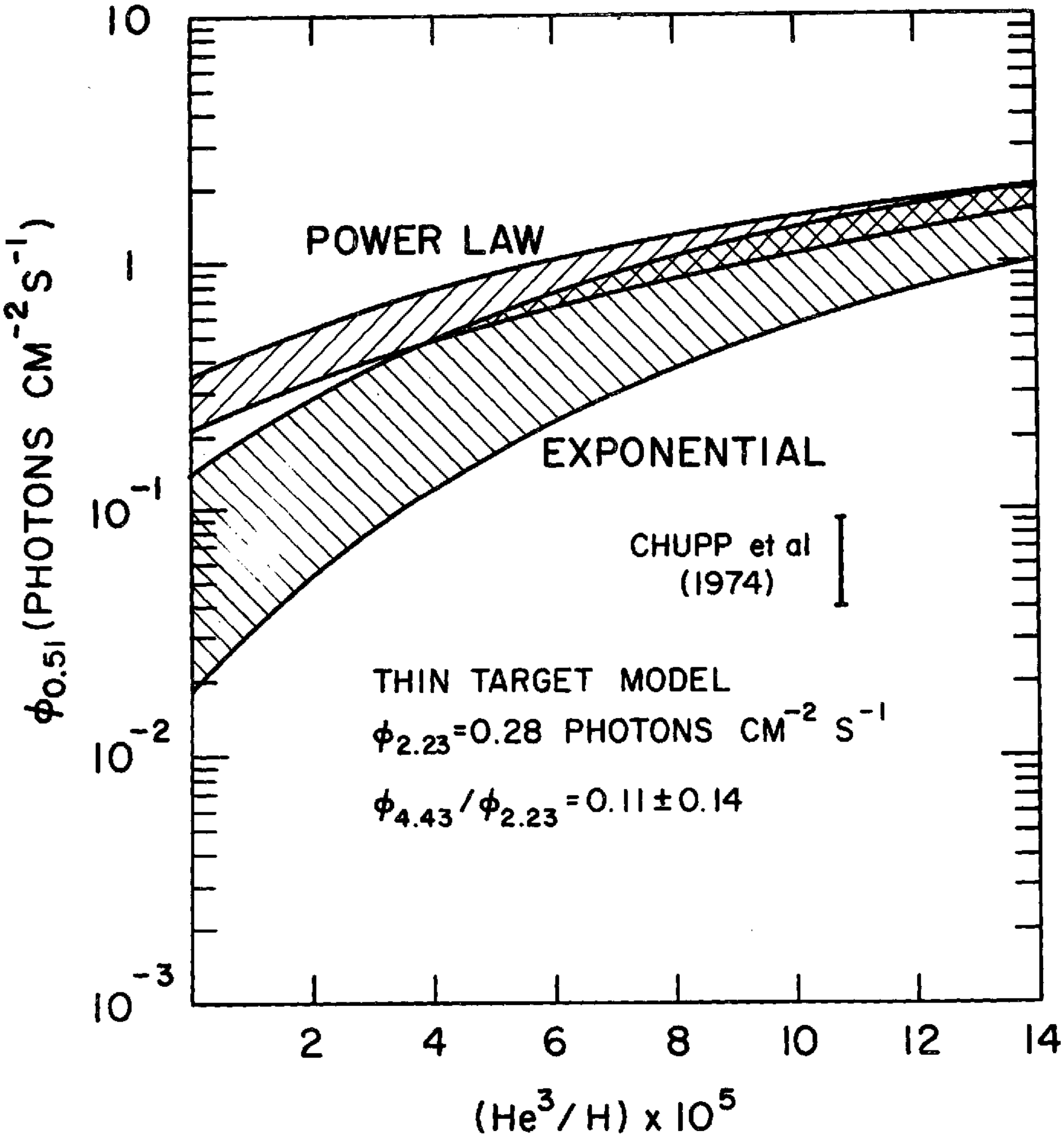
POWER LAW
EXPONENTIAL
CHUPP et al
(1974)
THIN TARGET MODEL
$\phi_{2.23}$=0.28 PHOTONS CM$^{-2}$ S$^{-1}$
$\phi_{4.43}/\phi_{2.23}$=0.11±0.14
$\phi_{0.51}$ (PHOTONS CM$^{-2}$ S$^{-1}$)
(He$^3$/H) x 10$^5$
10
1
10$^{-1}$
10$^{-2}$
10$^{-3}$
2
4
6
8
10
12
14

Figure 4

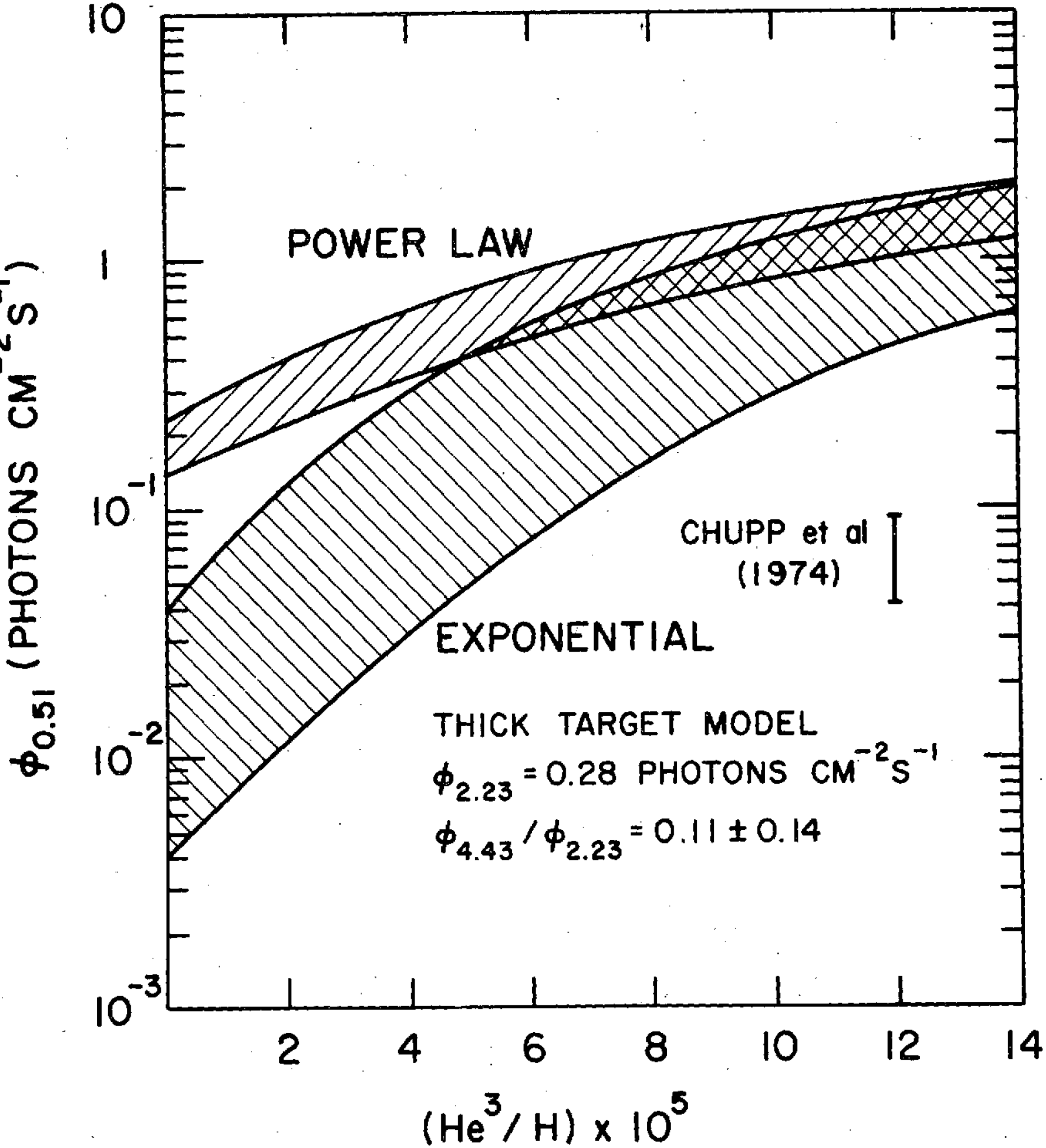

POWER LAW
EXPONENTIAL
CHUPP et al (1974)
THICK TARGET MODEL
$\phi_{2.23}$ = 0.28 PHOTONS $CM^{-2}S^{-1}$
$\phi_{4.43}/\phi_{2.23}$ = 0.11 ± 0.14
$\phi_{0.51}$ (PHOTONS $CM^{-2}S^{-1}$)
($He^3$/H) x $10^5$
10
1
$10^{-1}$
$10^{-2}$
$10^{-3}$
2
4
6
8
10
12
14


Figure 5

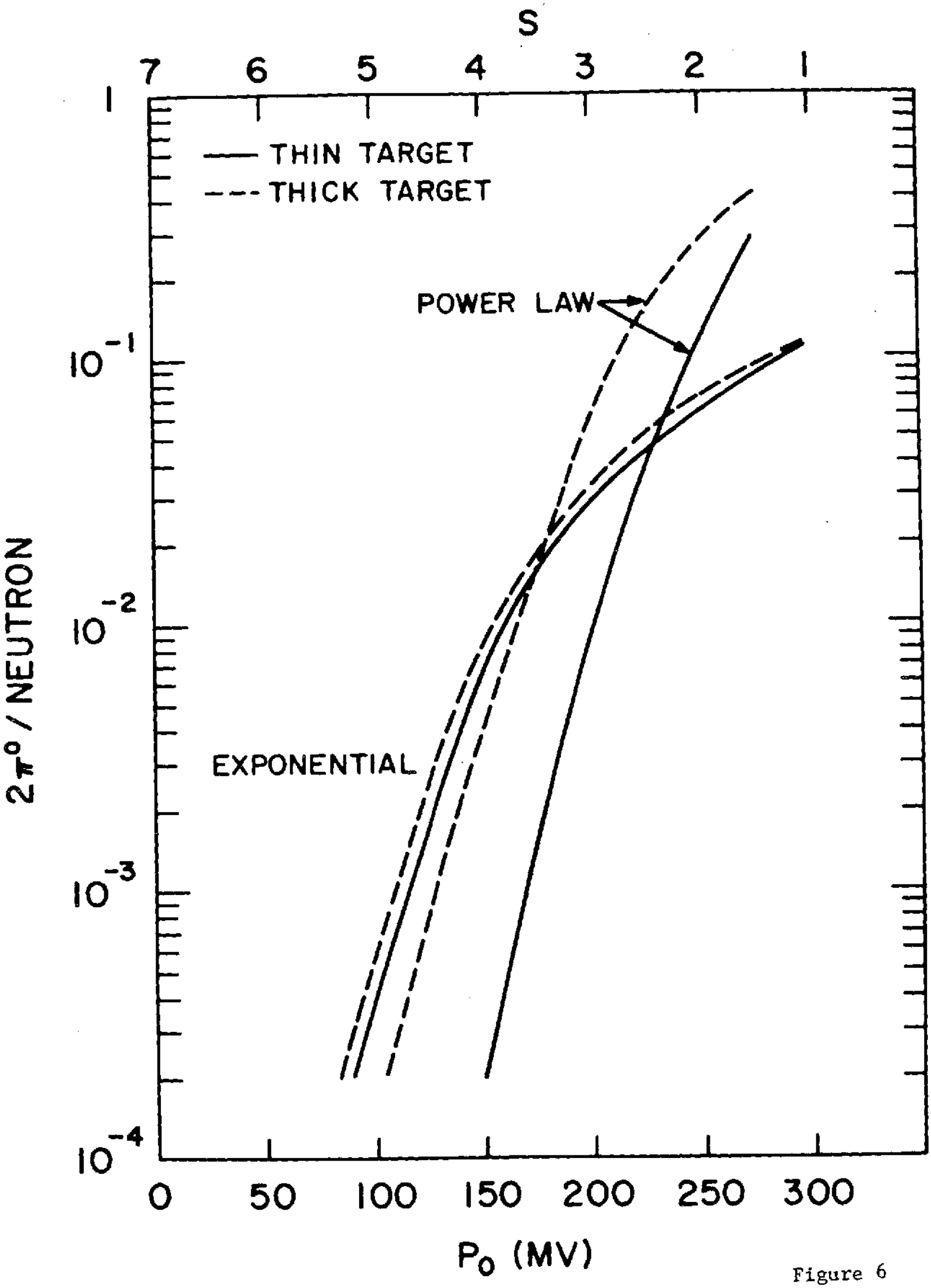

S
7
6
5
4
3
2
1
THIN TARGET
THICK TARGET
POWER LAW
EXPONENTIAL
$2\pi^0$ / NEUTRON
1
$10^{-1}$
$10^{-2}$
$10^{-3}$
$10^{-4}$
0
50
100
150
200
250
300
$P_0$ (MV)


Figure 6

REPRODUCIBILITY OF THE
ORIGINAL PAGE IS POOR

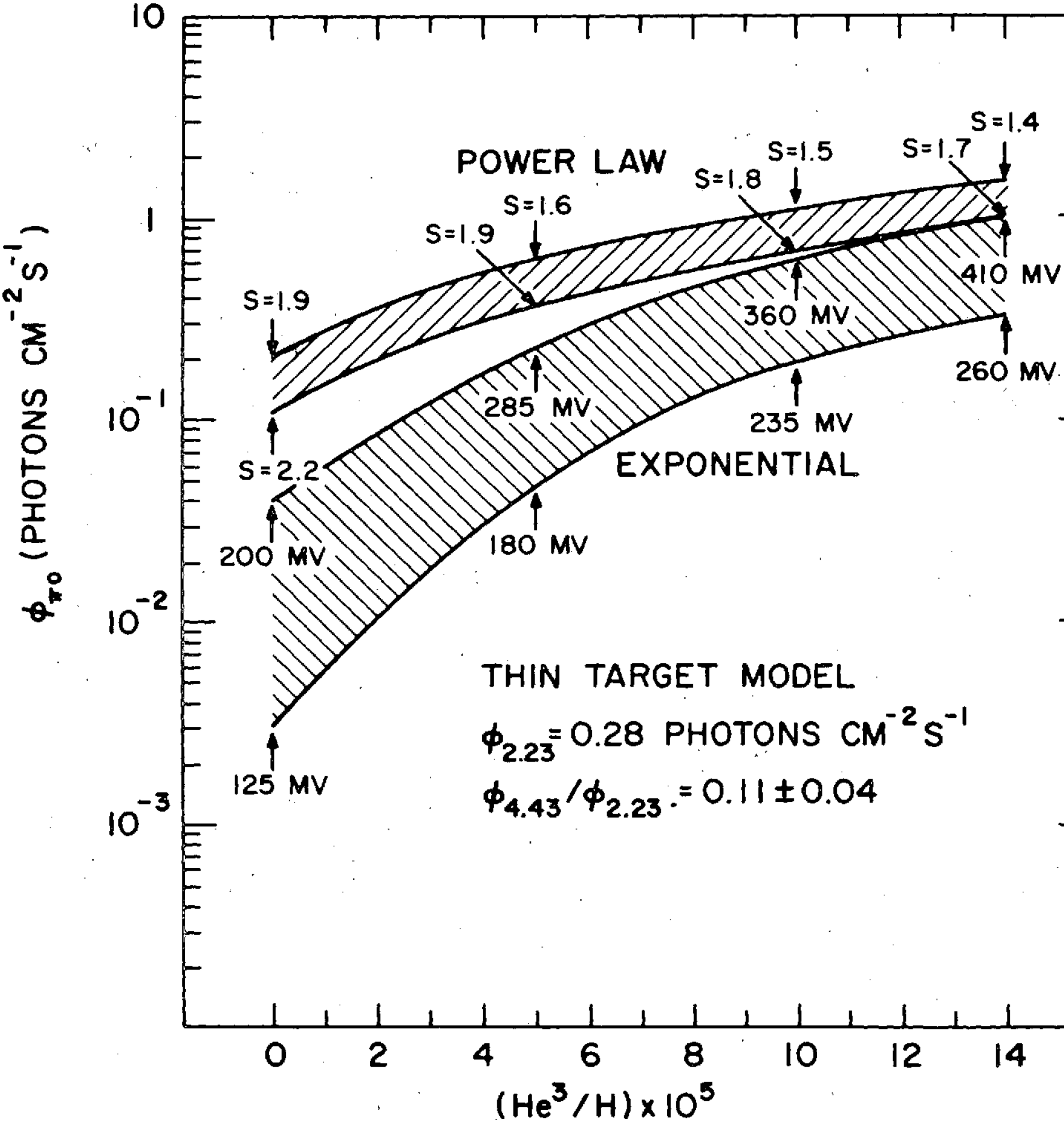


Figure 7

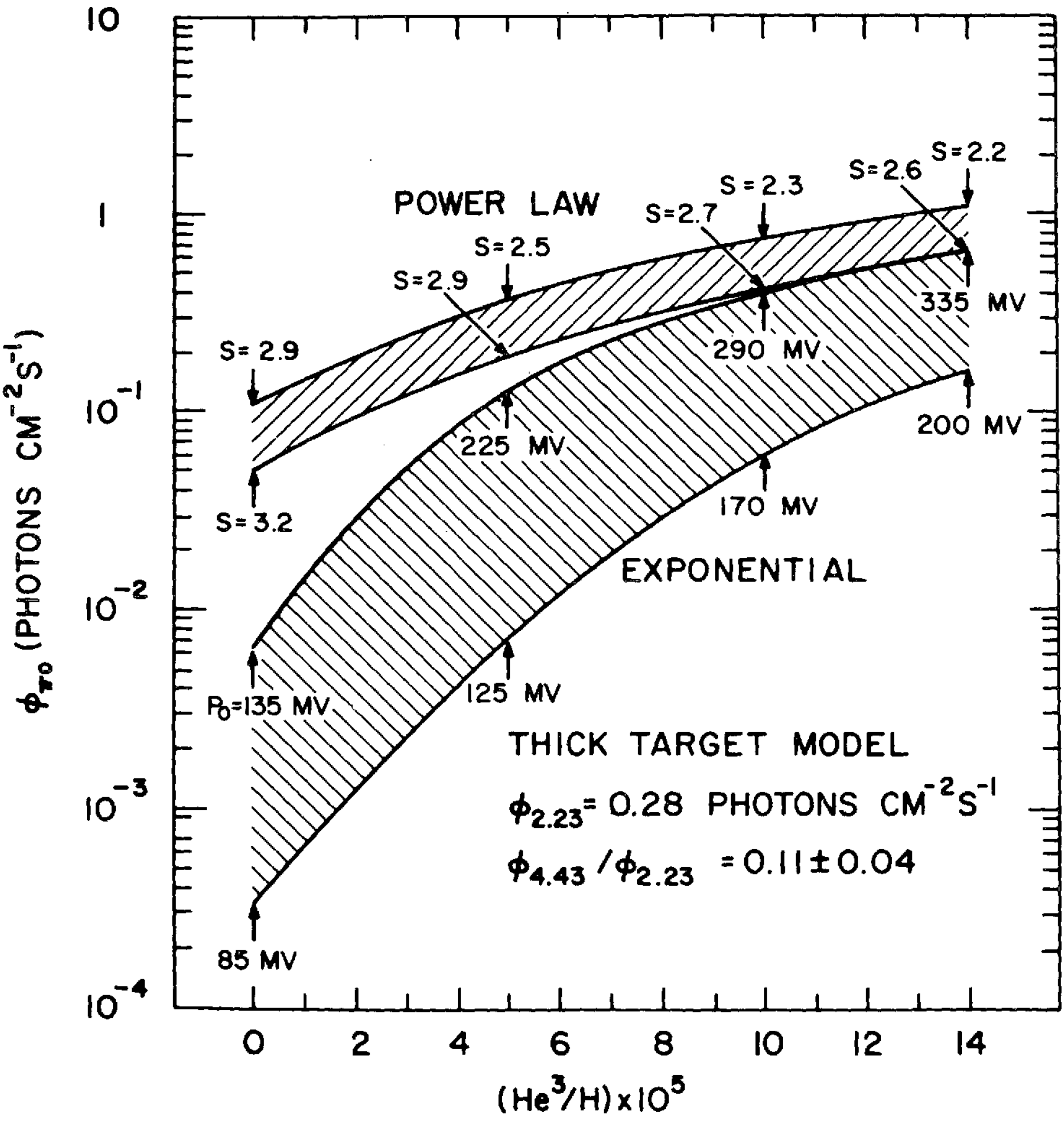

POWER LAW
S=2.9
S=2.9
S=2.5
S=2.7
S=2.3
S=2.6
S=2.2
S=3.2
335 MV
290 MV
225 MV
200 MV
170 MV
EXPONENTIAL
$P_0$=135 MV
125 MV
85 MV
THICK TARGET MODEL
$\phi_{2.23}$= 0.28 PHOTONS $CM^{-2}S^{-1}$
$\phi_{4.43}/\phi_{2.23}$ = 0.11 ± 0.04
$\phi_{\pi^0}$ (PHOTONS $CM^{-2}S^{-1}$)
($He^3$/H) x $10^5$


Figure 8

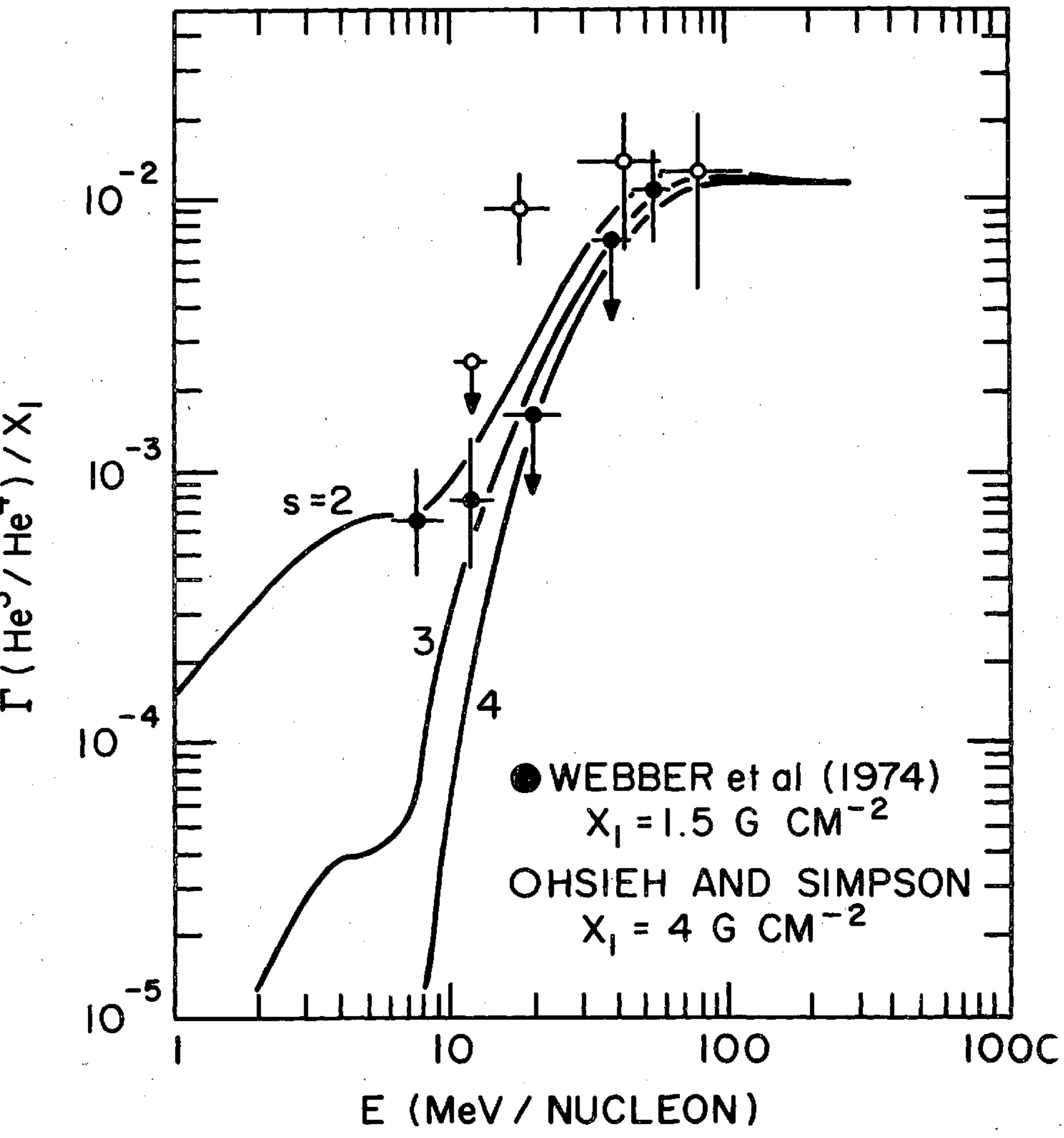

$10^{-2}$
$10^{-3}$
$10^{-4}$
$10^{-5}$
$\Gamma(He^3/He^4)/X_1$
s = 2
3
4
WEBBER et al (1974)
$X_1$ = 1.5 G CM$^{-2}$
OHSIEH AND SIMPSON
$X_1$ = 4 G CM$^{-2}$
1
10
100
1000
E (MeV / NUCLEON)


Figure 9

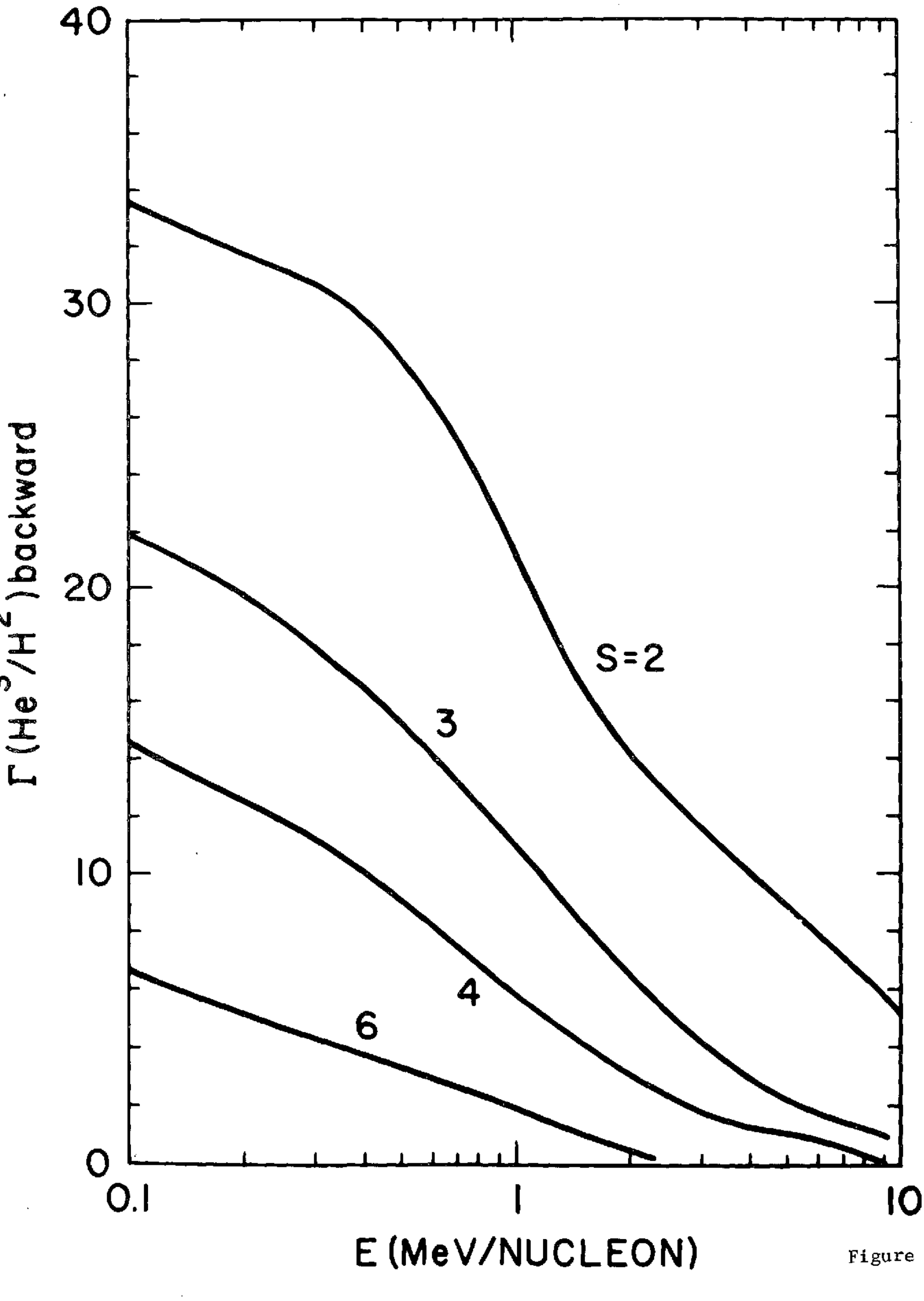


Figure 10

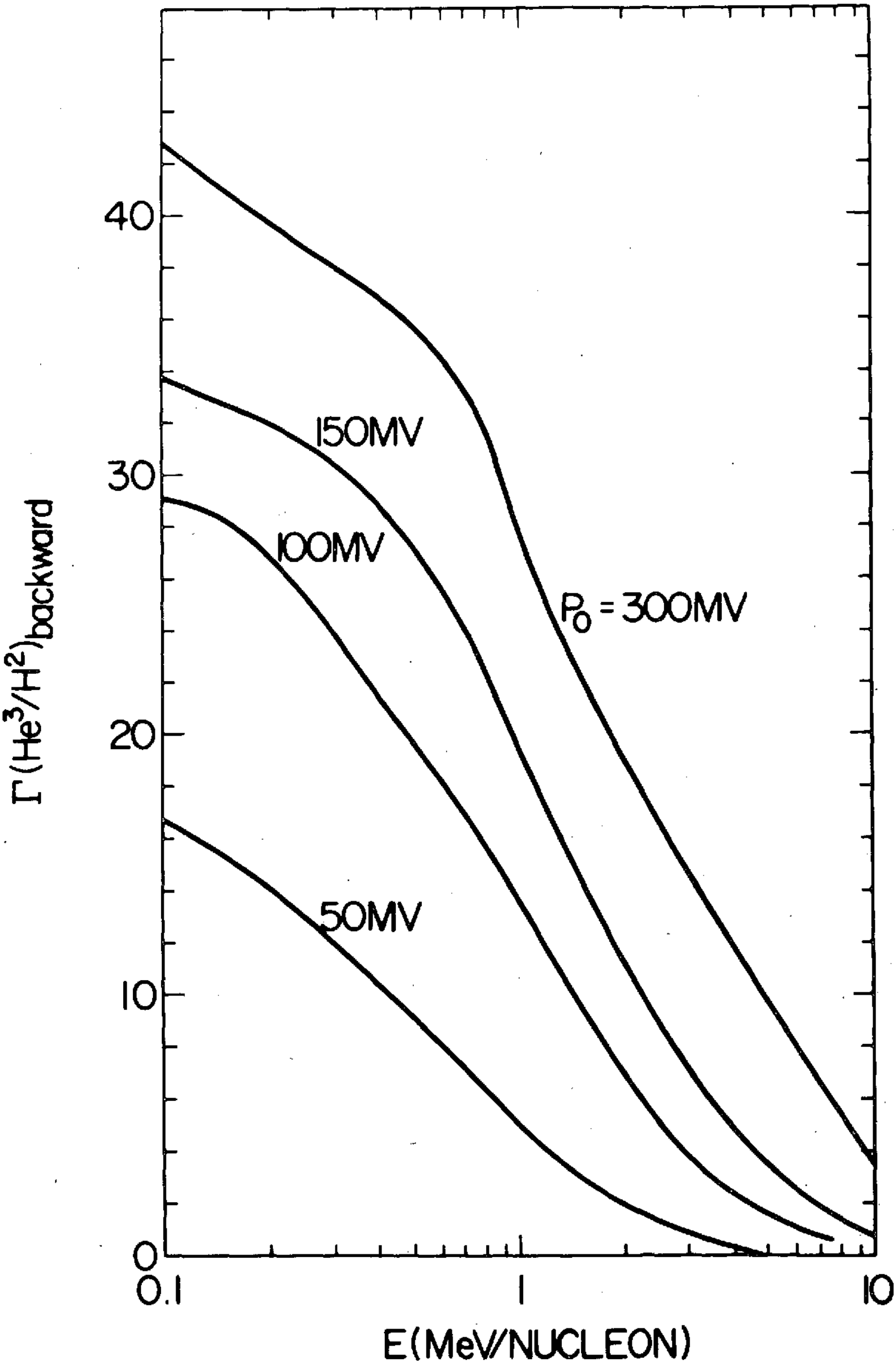
40
30
20
10
0
0.1
1
10
$\Gamma(He^3/H^2)_{backward}$
E(MeV/NUCLEON)
150MV
100MV
50MV
$P_0$ = 300MV

Figure 11